Optics Express, Vol. 22, Issue 21, pp. 25466-25480.

Objective speckle displacement: an extended theory for the small deformation of shaped objects

Thomas O. H. Charrett[*] and Ralph P. Tatam

Engineering Photonics, Cranfield University, MK43 0AL, UK
[*]*t.charrett@cranfield.ac.uk*

Abstract: This paper describes an extended and improved theory of the displacement of the objective speckle pattern resulting from displacement and/or deformation of a coherently illuminated diffuse object. Using the theory developed by Yamaguchi [Opt. Acta **28**, 1359 (1981)], extended expressions are derived that include the influence of surface shape/gradients via the first order approximation of the shape as linear surface gradients. Both the original Yamaguchi expressions and the extended form derived here are shown experimentally to break down as the detector position moves away from the *z*-axis. As such, improved forms of the expressions are then presented, which remove some of the approximations used by Yamaguchi and can be used to predict the objective speckle displacement over a wide range of detector positions and surface slopes. Finally, these expressions are then verified experimentally for the speckle shifts resulting from object translations.

©2014 Optical Society of America

OCIS codes: (030.6140) Speckle; (110.6150) Speckle imaging; (120.6150) Speckle imaging; (120.0120) Instrumentation, measurement, and metrology; (120.3940) Metrology.

References and links

1. I. Yamaguchi, "Speckle Displacement and Decorrelation in the Diffraction and Image Fields for Small Object Deformation," Opt. Acta **28**(10), 1359–1376 (1981).
2. H. Atcha and R. Tatam, "Heterodyning of fibre optic electronic speckle pattern interferometers using laser diode wavelength modulation," Meas. Sci. Technol. **5**, 704–709 (1994).
3. D. Francis, R. P. Tatam, and R. M. Groves, "Shearography technology and applications: a review," Meas. Sci. Technol. **21**(10), 102001 (2010).
4. L. Shirley and G. Hallerman, "Nonconventional 3D Imaging Using Wavelength-Dependent Speckle," Lincoln Lab. J. **9**, 153–186 (1996).
5. J. D. Briers and S. Webster, "Laser speckle contrast analysis (LASCA): a nonscanning, full-field technique for monitoring capillary blood flow," J. Biomed. Opt. **1**(2), 174–179 (1996).
6. S. Bianchi, "Vibration detection by observation of speckle patterns," Appl. Opt. **53**(5), 931–936 (2014).
7. I. Yamaguchi, "Automatic measurement of in-plane translation by speckle correlation using a linear image sensor," J. Phys. E. **19**, 944–948 (1986).
8. I. Yamaguchi and T. Fujita, "Laser speckle rotary encoder," Appl. Opt. **28**(20), 4401–4406 (1989).
9. I. Yamaguchi, "Advances in the laser speckle strain gauge," Opt. Eng. **27**(3), 273214 (1988).
10. I. Yamaguchi, K. Kobayashi, and L. Yaroslavsky, "Measurement of surface roughness by speckle correlation," Opt. Eng. **43**(11), 2753 (2004).
11. G. S. Spagnolo, D. Paoletty, and P. Zanetta, "Local speckle correlation for vibration analysis," Opt. Commun. **123**(1-3), 41–48 (1996).
12. P. Smíd, P. Horváth, and M. Hrabovský, "Speckle correlation method used to detect an object's surface slope," Appl. Opt. **45**(27), 6932–6939 (2006).
13. P. Horváth, P. Šmíd, P. Wagnerova, and M. Hrabovský, "Usage of a speckle correlation for object surface topography," Proc. SPIE **6034**, 603421 (2006).
14. T. O. H. Charrett, L. Waugh, and R. P. Tatam, "Speckle velocimetry for high accuracy odometry for a Mars exploration rover," Meas. Sci. Technol. **21**(2), 025301 (2010).
15. D. Francis, T. O. H. Charrett, L. Waugh, and R. P. Tatam, "Objective speckle velocimetry for autonomous vehicle odometry," Appl. Opt. **51**(16), 3478–3490 (2012).

#217014 - $15.00 USD Received 15 Jul 2014; revised 5 Sep 2014; accepted 15 Sep 2014; published 10 Oct 2014

16. P. Jacquot and P. K. Rastogi, "Speckle motions induced by rigid-body movements in freespace geometry: an explicit investigation and extension to new cases," Appl. Opt. **18**(12), 2022–2032 (1979).
17. J. Světlík, "Speckle Displacement: Two Related Approaches," J. Mod. Opt. **39**(1), 149–157 (1992).
18. M. Hrabovský, Z. Bača, and P. Horváth, "Theory of speckle displacement and decorrelation and its application in mechanics," Opt. Lasers Eng. **32**(4), 395–403 (1999).
19. P. Horváth, M. Hrabovský, and P. Šmíd, "Full theory of speckle displacement and decorrelation in the image field by wave and geometrical descriptions and its application in mechanics," J. Mod. Opt. **51**(5), 725–742 (2004).
20. I. Yamaguchi, "Speckle displacement for general object deformation of a curved surface," Proc. SPIE **8413**, 841307 (2012).
21. K. Briechle and U. D. Hanebeck, "Template matching using fast normalized cross correlation," Proc. SPIE **4387**, 95–102 (2001).
22. M. Raffel, C. Willert, S. Wereley, and J. Kompenhans, *Particle Image Velocimetry: A Practical Guide* (Springer, 2007).

1 Introduction

The properties of laser speckle are of great interest in many areas of non-contact optical instrumentation, including strain measurements, for example electronic speckle pattern interferometry (ESPI) [2] and shearography [3] as well as surface contouring [4], medicine [5] and vibration detection [6]. A particularly elegant measurement philosophy, termed speckle pattern correlation, relates the deformation of an illuminated object to the translation and de-correlation of its observed speckle pattern and was first described in the 1980's by Yamaguchi [1], who applied it to the measurement of object translation [7], rotation [8], strain [9] and surface roughness [10]. More recently, there has been renewed interest in the technique with researchers investigating new applications in industry, including vibration [11], surface slope [12], topology measurements [13] and robotic vehicle odometry [14,15]. In many of these applications knowledge of how the illuminated surface shape affects the observed speckle translation is of fundamental importance. For example, in robotic vehicle velocimetry systems a shaped surface has been observed to cause significant errors in the measured velocities.

Expressions for the speckle shift have in the past been derived by Jacquot [16], Yamaguchi [1] and later by Světlík [17] and Horvath *et al.* [18,19] and have varying degrees of complexity. Jacquot [16] used a method based upon the concept of homology, i.e. that given an initial point in the diffracted field, there exists a point where the amplitude is identical after the displacement of the object, while Yamaguchi [1,8] and others [17–19] used an approach based upon the cross-correlation of the speckle pattern intensities before and after deformation. Světlík [17] compared the results of these two approaches and presented an alternative cross-correlation based derivation to Yamaguchi's, that gives equivalent expressions to those found by Jacquot. More recently, Horvath *et al.* [18,19] have presented a more general and detailed derivation based on the method of Yamaguchi. However these present theories only address the limited cases of surfaces parallel to the detector plane, or for a cylindrical surface [8]. Yamaguchi [20] has also recently applied computer simulations in an attempt to model the speckle displacement from curved surfaces.

In this paper, the methodology of Yamaguchi is applied to extend the theory to include the influence of surface shape on the shift of the observed speckle pattern under deformation, via the approximation of the surface shape as first order surface gradients. A brief derivation of the theory developed by Yamaguchi [1] is presented in section 2. Then the same methodology and approximations are applied to give an extended theory that includes the influence of surface shape/gradients on the observed speckle shift. In section 3, experimental measurements of the translational scaling factors (the ratios of speckle shift to object translations) are presented and the expressions derived using Yamaguchi's approximations are shown to be only valid for on-axis detector positions. As a consequence, in section 4, improved expressions are derived, removing the need for some of the approximations used by Yamaguchi that are valid over a wider range of detector locations and include the influence of surface shape/gradients. Finally, further experimental measurements of the translational

#217014 - $15.00 USD Received 15 Jul 2014; revised 5 Sep 2014; accepted 15 Sep 2014; published 10 Oct 2014
(C) 2014 OSA

scaling factors are presented confirming the validity of these new expressions for various detector positions and surface gradient magnitudes and directions.

2 Speckle shift theory developed using Yamaguchi's approximations

For the general geometry shown in Fig. 1, a light source located at ***S***, illuminates the point ***R*** on the mean object surface, and the objective speckle pattern is observed by a detector at point ***D*** located at $z = L_0$.

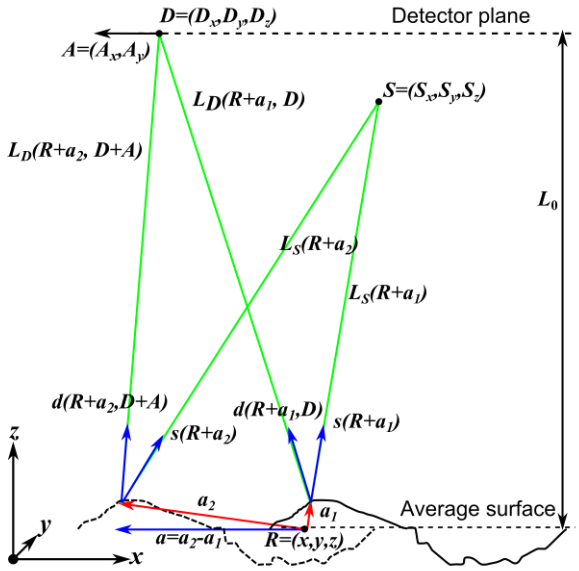


Fig. 1. General representation of the geometry used in the development of the speckle shift theory via cross-correlation of speckle intensities.

The intensity observed at the detector is given, in terms of the complex amplitude of the scattered light, $U(\boldsymbol{D})$, by $I(\boldsymbol{D}) = |U(\boldsymbol{D})|^2$ and the complex amplitudes of the scattered light before, $U_1(\boldsymbol{D}_1)$ and after deformation or displacement, $U_2(\boldsymbol{D}_2)$ can be written in terms of the path lengths as [1]:

$$U_n(\boldsymbol{D}_n) = \iint \sqrt{I_0\left(\boldsymbol{R} + \alpha_{Tn}(\boldsymbol{R})\right)}\,\zeta(\boldsymbol{R}) \exp(i\phi) \times \exp\left(ik\left[\left|\boldsymbol{L}_S(\boldsymbol{R}) - \boldsymbol{a}_n(\boldsymbol{R})\right| + \left|\boldsymbol{L}_D(\boldsymbol{R}, \boldsymbol{D}_n) - \boldsymbol{a}_n(\boldsymbol{R})\right|\right]\right) dxdy \quad (1)$$

Where the vectors, $\boldsymbol{L}_S(\boldsymbol{R})$ and $\boldsymbol{L}_D(\boldsymbol{R},\boldsymbol{D}_n)$ point from the mean object surface ***R*** to the light source ***S*** and observation point $\boldsymbol{D}_n$ respectively. The vector representing the displacement of the actual scattering surface from the mean object surface is given by $\boldsymbol{a}_n(\boldsymbol{R})$ and $I_0\left(\boldsymbol{R} + \alpha_{Tn}(\boldsymbol{R})\right)$ represents the intensity of the illuminating light at the surface point, where $\alpha_{Tn}(\boldsymbol{R})$ is the projection of $\boldsymbol{a}_n(\boldsymbol{R})$ onto the *x*-*y* plane. $\zeta(\boldsymbol{R})$ and $\exp(i\phi)$ are the macroscopic and microscopic reflection functions of the object and are related to the diffusing properties of the object [1] and *k* is the wavenumber.

Following the assumptions of Yamaguchi [1] that the displacement of the scattering surface is much smaller than the paths from the source to surface-point and surface-point to observation point, these can be approximated by:

#217014 - $15.00 USD Received 15 Jul 2014; revised 5 Sep 2014; accepted 15 Sep 2014; published 10 Oct 2014
(C) 2014 OSA

$$\begin{aligned}\left|\boldsymbol{L_S}\left(\boldsymbol{R}\right)-\boldsymbol{a_n}\left(\boldsymbol{R}\right)\right| &\approx L_S\left(\boldsymbol{R}\right)-\boldsymbol{a_n}\left(\boldsymbol{R}\right)\bullet\boldsymbol{s}\left(\boldsymbol{R}\right)\\ \left|\boldsymbol{L_D}\left(\boldsymbol{R},\boldsymbol{D_n}\right)-\boldsymbol{a_n}\left(\boldsymbol{R}\right)\right| &\approx L_D\left(\boldsymbol{R},\boldsymbol{D_n}\right)-\boldsymbol{a_n}\left(\boldsymbol{R}\right)\bullet\boldsymbol{d}\left(\boldsymbol{R},\boldsymbol{D_n}\right)\end{aligned} \tag{2}$$

Here, $\boldsymbol{s}(\boldsymbol{R})$ and $\boldsymbol{d}(\boldsymbol{R},\boldsymbol{D_n})$ are unit vectors in the direction of $\boldsymbol{L_S}(\boldsymbol{R})$ and $\boldsymbol{L_D}(\boldsymbol{R},\boldsymbol{D_n})$ respectively and $L_S(\boldsymbol{R})$ and $L_D(\boldsymbol{R},\boldsymbol{D_n})$ are the magnitudes. Substituting these expressions and $\boldsymbol{p}\left(\boldsymbol{R},\boldsymbol{D_n}\right)=\boldsymbol{s}\left(\boldsymbol{R}\right)+\boldsymbol{d}\left(\boldsymbol{R},\boldsymbol{D_n}\right)$ into Eq. (1) gives:

$$\begin{aligned}U_n\left(\boldsymbol{D_n}\right)=\iint\sqrt{I_0\left(\boldsymbol{R}+\alpha_{Tn}\left(\boldsymbol{R}\right)\right)}\exp\left(i\phi\right)\\ \times\exp\left(ik\left[L_S\left(\boldsymbol{R}\right)+L_D\left(\boldsymbol{R},\boldsymbol{D_n}\right)-\boldsymbol{a_n}\left(\boldsymbol{R}\right)\bullet\boldsymbol{p}\left(\boldsymbol{R},\boldsymbol{D_n}\right)\right]\right)dxdy\end{aligned} \tag{3}$$

An expression for the speckle shift resulting from a small object translation/deformation is then found from the cross-correlation function of the scattering intensities $I_1\left(\boldsymbol{D_1}\right)$ and $I_2\left(\boldsymbol{D}_2\right)$ at instances before and after the deformation which can be written as:

$$\left\langle I_1\left(\boldsymbol{D_1}\right)I_2^{\ *}\left(\boldsymbol{D_2}\right)\right\rangle=\left\langle\left|U_1\left(\boldsymbol{D_1}\right)\right|^2\right\rangle\left\langle\left|U_2\left(\boldsymbol{D}_2\right)\right|^2\right\rangle+\left|\left\langle U_1\left(\boldsymbol{D_1}\right)U_2^{\ *}\left(\boldsymbol{D_2}\right)\right\rangle\right|^2 \tag{4}$$

However, only the second term in Eq. (4) is of interest in determining the speckle shift, as this represents the cross-correlation function of the fluctuation of the intensity about the mean, i.e. the speckles. If the detector is originally located at $\boldsymbol{D_1} = \boldsymbol{D}$ then the maximum of this term will occur at the shifted detector position that corresponds to the speckle shift $\boldsymbol{A}$, i.e. $\boldsymbol{D_2} = \boldsymbol{D} + \boldsymbol{A}$. Replacing $\boldsymbol{D_1}$, $\boldsymbol{D_2}$ and setting $\alpha_{T1}(\boldsymbol{R}) = 0$, gives the following expression for the cross-correlation of the intensity fluctuations:

$$\begin{aligned}\left|\left\langle U_1\left(\boldsymbol{D_1}\right)U_2^{\ *}\left(\boldsymbol{D_2}\right)\right\rangle\right|=\iint\sqrt{I_0\left(\boldsymbol{R}\right)I_0\left(\boldsymbol{R}+\alpha_{T2}\left(\boldsymbol{R}\right)\right)}\\ \times\exp\left(ik\begin{bmatrix}L_D\left(\boldsymbol{R},\boldsymbol{D}\right)-L_D\left(\boldsymbol{R},\boldsymbol{D}+\boldsymbol{A}\right)\\ -\boldsymbol{p}\left(\boldsymbol{R},\boldsymbol{D}\right)\bullet\boldsymbol{a}_1\left(\boldsymbol{R}\right)+\boldsymbol{p}\left(\boldsymbol{R},\boldsymbol{D}+\boldsymbol{A}\right)\bullet\boldsymbol{a}_2\left(\boldsymbol{R}\right)\end{bmatrix}\right)dxdy\end{aligned} \tag{5}$$

Yamaguchi [1] then uses the assumption that for small displacements and neglecting higher terms the following can be substituted:

$$\begin{aligned}-\boldsymbol{p}\left(\boldsymbol{R},\boldsymbol{D}\right)\bullet\boldsymbol{a}_1\boldsymbol{R}+\boldsymbol{p}\left(\boldsymbol{R},\boldsymbol{D}+\boldsymbol{A}\right)\bullet\boldsymbol{a}_2\left(\boldsymbol{R}\right)&\approx\boldsymbol{p}\left(\boldsymbol{R},\boldsymbol{D}\right)\bullet\left(\boldsymbol{a}_2\left(\boldsymbol{R}\right)-\boldsymbol{a}_1\left(\boldsymbol{R}\right)\right)\\ &=\boldsymbol{p}\left(\boldsymbol{R},\boldsymbol{D}\right)\bullet\boldsymbol{a}\left(\boldsymbol{R}\right)\end{aligned} \tag{6}$$

Where $\boldsymbol{a}(\boldsymbol{R}) = \boldsymbol{a_2}(\boldsymbol{R}) - \boldsymbol{a_1}(\boldsymbol{R})$ is the net displacement of the surface point occurring during the deformation. By assuming the displacement/deformation is homogeneous within the illuminated region and can be approximated at the centre point, the Taylor expansion about $\boldsymbol{R}=0$ can be used, again ignoring terms higher than first order.

$$\boldsymbol{p}\left(\boldsymbol{R},\boldsymbol{D}\right)\bullet\boldsymbol{a}\left(\boldsymbol{R}\right)=\boldsymbol{p}\left(0,\boldsymbol{D}\right)\bullet\boldsymbol{a}\left(0\right)+\left[\nabla\boldsymbol{p}\left(\boldsymbol{R},\boldsymbol{D}\right)\bullet\boldsymbol{a}\left(\boldsymbol{R}\right)\right]_0\bullet\boldsymbol{R} \tag{7}$$

Finally, Yamaguchi uses a parabolic approximation to approximate the $L_D(\boldsymbol{R},\boldsymbol{D})$ and $L_D(\boldsymbol{R},\boldsymbol{D} + \boldsymbol{A})$ terms:

$$\begin{aligned}L_D\left(\boldsymbol{R},\boldsymbol{D}\right)&=L_0+\frac{\left|\boldsymbol{R}-\boldsymbol{D}\right|^2}{2L_0}\\ L_D\left(\boldsymbol{R},\boldsymbol{D}+\boldsymbol{A}\right)&=L_0+\frac{\left|\boldsymbol{R}-\boldsymbol{D}-\boldsymbol{A}\right|^2}{2L_0}\end{aligned} \tag{8}$$

#217014 - $15.00 USD Received 15 Jul 2014; revised 5 Sep 2014; accepted 15 Sep 2014; published 10 Oct 2014
(C) 2014 OSA

Applying the assumptions given in Eqs. (6)-(8) yields:

$$\begin{aligned}\left|\left\langle U_1(\boldsymbol{D_1})U_2^*(\boldsymbol{D_2})\right\rangle\right| &= \exp\left(ik\left[\frac{\boldsymbol{DA}}{L_0} - \boldsymbol{p}(0,\boldsymbol{D})\bullet\boldsymbol{a}_1(0)\right]\right)\\ &\times\iint\sqrt{I_0(\boldsymbol{R})I_0\left(\boldsymbol{R}+\alpha_{T2}(\boldsymbol{R})\right)}\\ &\times\exp\left(ik\left[\boldsymbol{A}+L_0\left[\nabla\boldsymbol{p}(\boldsymbol{R},\boldsymbol{D})\bullet\boldsymbol{a}(\boldsymbol{R})\right]_0\right]\frac{\boldsymbol{R}}{L_0}\right)dxdy\end{aligned} \tag{9}$$

From this it can be seen that the cross-correlation function will be a maximum where the second exponential term is zero, hence:

$$\boldsymbol{A} = -L_0\left[\nabla\boldsymbol{p}(\boldsymbol{R},\boldsymbol{D})\bullet\boldsymbol{a}(\boldsymbol{R})\right]_0 \tag{10}$$

This can be expanded in terms of the partial derivatives, and the derivatives of $\boldsymbol{a}$ further expressed in terms of the components of the strain tensor and rotation vector:

$$\begin{aligned}&\frac{\delta a_x}{\delta x} = \varepsilon_{xx} && \frac{\delta a_y}{\delta y} = \varepsilon_{yy} && \frac{1}{2}\left(\frac{\delta a_x}{\delta y}+\frac{\delta a_y}{\delta x}\right) = \varepsilon_{xy} = \varepsilon_{yx}\\ &\frac{\delta a_z}{\delta y} = \Omega_x && -\frac{\delta a_z}{\delta x} = \Omega_y && \frac{1}{2}\left(\frac{\delta a_y}{\delta x}-\frac{\delta a_x}{\delta y}\right) = \Omega_z\end{aligned} \tag{11}$$

Giving in matrix form:

$$\begin{aligned}\begin{bmatrix}A_x\\A_y\end{bmatrix} &= [T]\begin{bmatrix}a_x\\a_y\\a_z\end{bmatrix} + [R]\begin{bmatrix}\Omega_x\\\Omega_y\\\Omega_z\end{bmatrix} + [D]\begin{bmatrix}\varepsilon_{xx}\\\varepsilon_{xy}\\\varepsilon_{yy}\end{bmatrix}\\ [T] &= -L_0\begin{bmatrix}\frac{\delta(s_x+d_x)}{\delta x} & \frac{\delta(s_y+d_y)}{\delta x} & \frac{\delta(s_z+d_z)}{\delta x}\\ \frac{\delta(s_x+d_x)}{\delta y} & \frac{\delta(s_y+d_y)}{\delta y} & \frac{\delta(s_z+d_z)}{\delta y}\end{bmatrix}\\ [R] &= -L_0\begin{bmatrix}0 & -(s_z+d_z) & (s_y+d_y)\\ -(s_z+d_z) & 0 & -(s_x+d_x)\end{bmatrix}\\ [D] &= -L_0\begin{bmatrix}(s_x+d_x) & (s_y+d_y) & 0\\ 0 & (s_x+d_x) & (s_y+d_y)\end{bmatrix}\end{aligned} \tag{12}$$

Where the matrices [*T*], [*R*], and [*D*] give the coefficients relating the speckle pattern translation, A_x and A_y, to surface translations, rotations and strains respectively.

2.1 Speckle shift for a surface lying in the xy-plane

For the case described by Yamaguchi [1] and Horvath *et al.* [19], only diffuse surfaces with the mean surface lying in the *xy*-plane are considered. The expressions governing the speckle shift in these cases can then be found by setting; $\boldsymbol{S} = (S_x,S_y,S_z)$, $\boldsymbol{R} = (x,y,0)$, and $\boldsymbol{D} = (D_x,D_y,D_z)$ then computing the partial derivatives required in Eq. (12):

#217014 - $15.00 USD Received 15 Jul 2014; revised 5 Sep 2014; accepted 15 Sep 2014; published 10 Oct 2014
(C) 2014 OSA

$$\frac{\delta \boldsymbol{s}}{\delta x}=\frac{1}{L_S}\left(s_x{}^2-1,\quad s_x s_y,\quad s_x s_z\right) \qquad \frac{\delta \boldsymbol{s}}{\delta y}=\frac{1}{L_S}\left(s_x s_y,\quad s_y{}^2-1,\quad s_y s_z\right)$$
$$\frac{\delta \boldsymbol{d}}{\delta x}=\frac{1}{L_D}\left(d_x{}^2-1,\quad d_x d_y,\quad d_x d_z\right) \qquad \frac{\delta \boldsymbol{d}}{\delta y}=\frac{1}{L_D}\left(d_x d_y,\quad d_y{}^2-1,\quad d_y d_z\right) \tag{13}$$

Substituting these into the expression for [*T*] and applying $L_D \sim L_0$ gives the final result for the speckle shift due to translations:

$$[T]=-L_0\begin{bmatrix}\frac{\left(s_x{}^2-1\right)}{L_S}+\frac{\left(d_x{}^2-1\right)}{L_0} & \frac{\left(s_x s_y\right)}{L_S}+\frac{\left(d_x d_y\right)}{L_0} & \frac{\left(s_x s_z\right)}{L_S}+\frac{\left(d_x d_z\right)}{L_0}\\ \frac{\left(s_x s_y\right)}{L_S}+\frac{\left(d_x d_y\right)}{L_0} & \frac{\left(s_y{}^2-1\right)}{L_S}+\frac{\left(d_y{}^2-1\right)}{L_0} & \frac{\left(s_y s_z\right)}{L_S}+\frac{\left(d_y d_z\right)}{L_0}\end{bmatrix} \tag{14}$$

Equation (12) and the matrices [*T*],[*R*], and [*D*] defined above correspond to the Eqs. given by Yamaguchi [1], and later Horvath and Hrabovsky [18,19].

2.2 Extended equations for the speckle shift for a shaped/sloped surface

To extend the theory to include the influence of mean surface shape, the surface can be approximated by the linear surface gradients $m_x=\delta z/\delta x, m_y=\delta z/\delta y$ of the surface. Hence the surface points can now be written as, $\boldsymbol{R}$ = (x,y, $m_x x + m_y y$) and the partial derivatives are now:

$$\begin{aligned}
\frac{\delta \boldsymbol{s}}{\delta x}&=\frac{1}{L_S}\left(m_x s_x s_z+s_x{}^2-1,\quad m_x s_y s_z+s_x s_y,\quad m_x\left(s_z{}^2-1\right)+s_x s_z\right)\\
\frac{\delta \boldsymbol{s}}{\delta y}&=\frac{1}{L_S}\left(m_y s_x s_z+s_x s_y,\quad m_y s_y s_z+s_y{}^2-1,\quad m_y\left(s_z{}^2-1\right)+s_y s_z\right)\\
\frac{\delta \boldsymbol{d}}{\delta x}&=\frac{1}{L_D}\left(m_x d_x d_z+d_x{}^2-1,\quad m_x d_y d_z+d_x d_y,\quad m_x\left(d_z{}^2-1\right)+d_x d_z\right)\\
\frac{\delta \boldsymbol{d}}{\delta y}&=\frac{1}{L_D}\left(m_y d_x d_z+d_x d_y,\quad m_y d_y d_z+d_y{}^2-1,\quad m_y\left(d_z{}^2-1\right)+d_y d_z\right)
\end{aligned} \tag{15}$$

By substituting the modified partial derivatives into Eq. (12) and rearranging, an expression for the speckle shift of a shaped object approximated by its linear surface gradients can then be found:

$$\begin{bmatrix}A_x\\A_y\end{bmatrix}=\left([T]+[T']\right)\begin{bmatrix}a_x\\a_y\\a_z\end{bmatrix}+[R]\begin{bmatrix}\Omega_x\\\Omega_y\\\Omega_z\end{bmatrix}+[D]\begin{bmatrix}\varepsilon_{xx}\\\varepsilon_{xy}\\\varepsilon_{yy}\end{bmatrix} \tag{16}$$

Where:

$$[T']=-L_0\begin{bmatrix}m_x\left(\frac{s_x s_z}{L_S}+\frac{d_x d_z}{L_D}\right) & m_x\left(\frac{s_y s_z}{L_S}+\frac{d_y d_z}{L_D}\right) & m_x\left(\frac{\left(s_z{}^2-1\right)}{L_S}+\frac{\left(d_z{}^2-1\right)}{L_D}\right)\\ m_y\left(\frac{s_x s_z}{L_S}+\frac{d_x d_z}{L_D}\right) & m_y\left(\frac{s_y s_z}{L_S}+\frac{d_y d_z}{L_D}\right) & m_y\left(\frac{\left(s_z{}^2-1\right)}{L_S}+\frac{\left(d_z{}^2-1\right)}{L_D}\right)\end{bmatrix}$$

#217014 - $15.00 USD Received 15 Jul 2014; revised 5 Sep 2014; accepted 15 Sep 2014; published 10 Oct 2014
(C) 2014 OSA

Here [*T'*] is a matrix relating surface gradients to the additional speckle shift due to surface translations and the matrices [*T*], [*R*], and [*D*] remain unchanged from the standard Yamaguchi derivation given by Eqs. (12) and (14)

3 Validity of the Yamaguchi approximations

To experimentally test the above relations, an experimental system was constructed using an aluminum profile support structure above a test object mounted on a translation stage positioned in the *xy*-plane at z = 0mm. The three-dimensional support structure allowed the positions of the laser source and camera to be varied over a wide range of geometries (~ ± 80mm in *x*,*y* and up to 400mm in *z*) that are typical of practical applications of the speckle correlation method such as speckle velocimetry [14,15]. The test objects used were custom 3D printed ramps with gradients of 0.0 (flat), 0.2, 0.4, 0.6, 0.8 and 1.0 (45° slope) as shown in Fig. 2. The ramps were constructed with an octagonal cross-section allowing the gradients to be rotated in 45° increments to vary both components of the surface gradient in a controlled manner. The quoted precision of the 3D printing process was ± 0.1mm over a ramp dimension of 30mm giving a precision of the gradients of ± 0.003. The translation stage used in this work was a Physik Instrumente M-110.1DG linear translation stage with a quoted unidirectional repeatability of 0.1µm. The camera was a Baumer HXC-13 CMOS camera with 14x14µm pixels. A laser line filter was located in front of the camera sensor to block background light and ensure high contrast speckle images. The laser source used was a diode-pumped solid state (DPSS) laser module producing approximately 30mW at 532nm. The collimated output of the laser was expanded onto the surface of the test object using an f = 45mm lens to produce a speckle size of around 5 pixels on the camera.

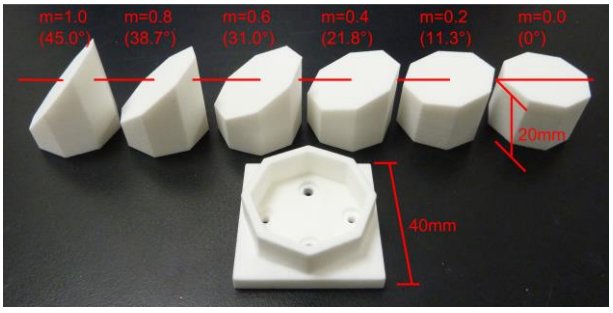


Fig. 2. The 3D printed test objects used in this experiment. From left to right $m_{x,y}$ = 1.0, 0.8, 0.6, 0.4, 0.2 and 0.0 and the stage mounting plate. The ramps have a constant working height of 20mm above the stage at the centre point and can be rotated in 45° increments in the mounting plate to enable the surface gradient direction to be rotated in a controlled manner.

The translational scaling factors (ratios of speckle shift to object translation), A_x/a_x, A_x/a_y, A_x/a_z and A_y/a_x, A_y/a_y, A_y/a_z, were experimentally measured by recording images before and after a known translation. The normalized cross-correlation [21] was computed and a Gaussian peak fitting [14] was performed to locate the peak and determine the speckle shift to 0.1 pixel accuracy (1.4µm). This was repeated 10 times and the mean speckle shift was recorded for each object translation. This was then performed over a range of stage translations from 0 to 500 µm to avoid pixel locking [22] and/or stage positional bias errors, such as caused by unwanted stage roll, pitch or yaw, with the final translational scaling factor being determined by a linear fit to these recorded mean shifts. This allowed the scaling factors to be determined to within an estimated accuracy of ± 0.02. To improve the accuracy further, it would be necessary to carefully align the detector and stages axis to better than then current estimated 0.5° accuracy. This is because any misalignment will cause translations in the other two orthogonal components, resulting in an unwanted contribution to speckle shift. This angular misalignment comes from both misalignment of the stage with the support structure,

#217014 - $15.00 USD Received 15 Jul 2014; revised 5 Sep 2014; accepted 15 Sep 2014; published 10 Oct 2014
(C) 2014 OSA

which is constant, and from misalignment of the camera and support structure which can vary each time the camera is repositioned and was estimated at 0.5° by measurement of the length and transverse displacement possible when fixing the mounting brackets. The repeatability of the measurements of the scaling factors is approximately ± 0.008, and is limited by the pixel size of the detector and the 0.1 pixel peak fitting accuracy.

When the experimental results were compared to the values predicted by the original Yamaguchi theory, Eq. (14), and the new extended equations given in Eq. (16), it was observed that both theories fail to accurately predict the speckle shift behavior when the detector is located away from the *z*-axis. For example, in Fig. 3 the measured speckle shift translational scaling factors are shown for a source located at $\boldsymbol{S}$ = (0,-150,265) mm and various detector positions along the *x*-axis, $\boldsymbol{D}$ = (D_x,0,300)mm and for three surface gradients,(a) $m_x = 0$, $m_y = 0$, the case modelled by Yamaguchi and others, and (b) and (c) for the $m_x = \pm 1$, $m_y = 0$ cases. In the case of zero surface gradients a divergence between the observed (data points) and predicted (solid lines) scaling factors can be seen as the detector location is moved away from the z-axis. This divergence is most noticeable in the A_x/a_x, A_y/a_y components and is further accentuated when the influence of surface gradients is included in the extended theory.

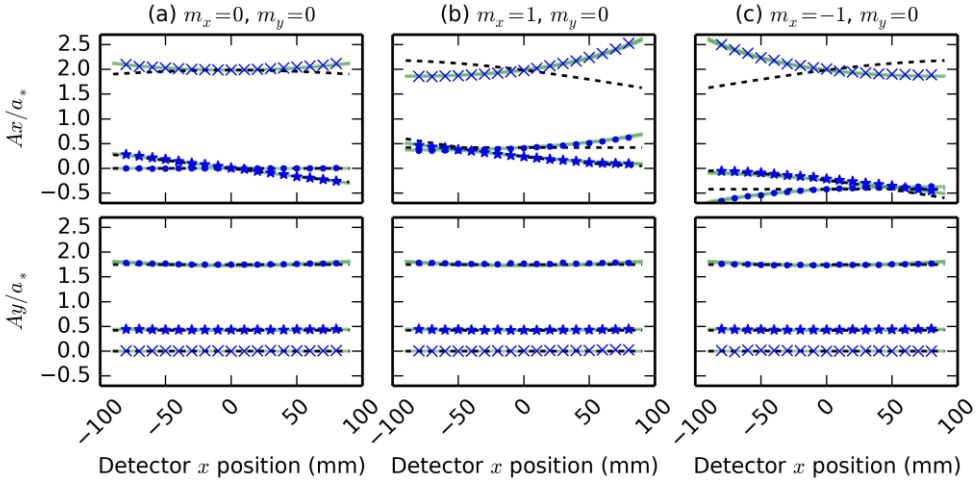


Fig. 3. Comparison of measured and theoretical translational scaling factors for a source and detector positioned at $\boldsymbol{S}$ = (0,-150,265) mm and $\boldsymbol{D}$ = (D_x,0,300) mm, for three surface gradients (a) $m_x = m_y = 0$; (b) $m_x = +1$, $m_y = 0$ and (c) $m_x = -1$, $m_y = 0$. The top row shows the scaling factors for the speckle shift in the *x* direction (A_x) resulting from the object translations (a_x, a_y and a_z) while the bottom row shows scaling factors for the speckle shift in the y direction (A_y). The data points are the experimental results; (✖) $A_{x,y}/a_x$, (●) $A_{x,y}/a_y$ and (★) $A_{x,y}/a_z$, and the dashed lines shows the values predicted by the Yamaguchi's equations (for $m_x = m_y = 0$) and the extended equations presented in section 2. The solid lines (green) are the values predicted by the improved equations presented in section 4. Here the thickness of the line denotes the minimum and maximum bounds predicted assuming an error in source and detector positions of ± 1mm in all directions.

This divergence from the theory has also been noted by Světlík [17] although this work does not appear to be widely known about or cited. Indeed Světlík derives an alternative form of the equations, using a similar but different cross-correlation approach where the correlation function is approximated by a delta function. These successfully predict the speckle translations over a wider range of detector positions for the zero-gradient case and agree with those found by Jacquot [16] using a method based upon the concept of homology. An improved version of the speckle shift equations that can be used to predict the speckle shift at other detector locations can be found, in a different manner, by modifying Yamaguchi's

#217014 - $15.00 USD Received 15 Jul 2014; revised 5 Sep 2014; accepted 15 Sep 2014; published 10 Oct 2014
(C) 2014 OSA

approximations. This is presented in section 4 along with an extended form taking into account surface gradients.

However the extended equations, presented in section 2.2 using Yamaguchi's approximations, are still applicable when the detector is located at the *z*-axis (i.e. $\underline{D_x} = D_y = 0$). Figure 4 shows the measured translational scaling factors for a detector located at $\boldsymbol{D}$ = (0,0,300)mm and a source located at $\boldsymbol{S}$ = (0,-150,265)mm and shows the scaling factors compared to the theoretical values predicted by Eqs. (12) and (16). In Fig. 4 (a), the *x* surface gradient is varied between $m_x = -1.0$ to + 1.0 with $m_y = 0$. The solid lines represent the values predicted by the extended theory. Figure 4 (b) shows the same, but with varying m_y with m_x fixed. Finally, Fig. 4 (c) shows the scaling factors obtained for varying direction of a fixed magnitude gradient as it is rotated about the *z*-axis ($m_x = \cos\phi$, $m_y = -\sin\phi$). It can be seen that there is good agreement between the predicted and experimental values, for a wide range of gradient magnitudes and directions.

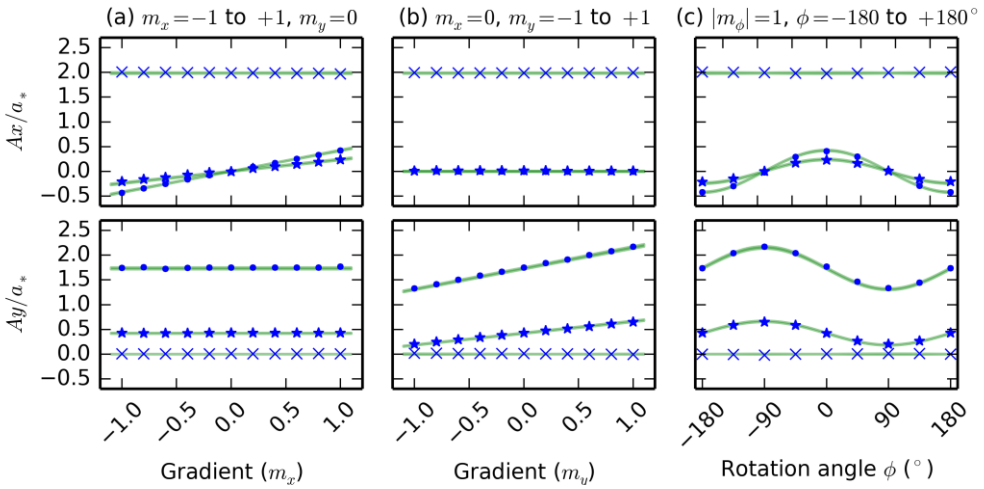


Fig. 4. Comparison of measured and theoretical translational scaling factors for a source at $\boldsymbol{S}$ = (0,-150,265) mm, and the detector positioned on the *z*-axis at $\boldsymbol{D}$ = (0,0,300) mm, for varying surface gradients; (a) for varying m_x; (b) for varying m_y and (c) for varying directions of a fixed magnitude gradient as it is rotated about the *z*-axis ($m_x = \cos\phi$, $m_y = -\sin\phi$). The top row shows the scaling factors for the speckle shift in the *x* direction (A_x) resulting from the object translations (a_x, a_y and a_z) while the bottom row shows scaling factors for the speckle shift in the *y* direction (A_y). The data points are the experimentally measured results; (✖) $A_{x,y}/a_x$, (●) $A_{x,y}/a_y$ and (★) $A_{x,y}/a_z$, and the solid lines show the values predicted by both the extended equations (section 2) and the improved equations (section 4), which are identical when the detector is located on the *z*-axis. Here the thickness of the line denotes the minimum and maximum bounds predicted assuming an error in source and detector positions of ± 1mm in all directions.

4 Improved speckle shift equations for detector positions where $(D_x, D_y) \neq (0,0)$

As demonstrated in section 3, the existing theory breaks down for measurement geometries where the detector is moved away from the *z*-axis. To address this, an improved theory with wider validity was developed. By starting from the expressions for the complex amplitudes $U_n(\boldsymbol{D_n})$ given by Eq. (1) where $\boldsymbol{D_1} = \boldsymbol{D}$ and $\boldsymbol{D_2} = \boldsymbol{D} + \boldsymbol{A}$ and remembering that a shift in the detector position is equivalent to a shift of the surface in the opposite direction, the paths from the source to surface-point and surface-point to observation points before and after the deformation can now be approximated by:

#217014 - $15.00 USD Received 15 Jul 2014; revised 5 Sep 2014; accepted 15 Sep 2014; published 10 Oct 2014
(C) 2014 OSA

$$
\begin{aligned}
&\left|\boldsymbol{L_S}\left(\boldsymbol{R}\right)-\boldsymbol{a}_1\left(\boldsymbol{R}\right)\right| \approx L_S\left(\boldsymbol{R}\right)-\boldsymbol{a}_1\left(\boldsymbol{R}\right)\bullet\boldsymbol{s}\left(\boldsymbol{R}\right)\\
&\left|\boldsymbol{L_S}\left(\boldsymbol{R}\right)-\boldsymbol{a}_2\left(\boldsymbol{R}\right)\right| \approx L_S\left(\boldsymbol{R}\right)-\boldsymbol{a}_2\left(\boldsymbol{R}\right)\bullet\boldsymbol{s}\left(\boldsymbol{R}\right)\\
&\left|\boldsymbol{L}_D\left(\boldsymbol{R},\boldsymbol{D}\right)-\boldsymbol{a}_1\left(\boldsymbol{R}\right)\right| \approx L_D\left(\boldsymbol{R},\boldsymbol{D}\right)-\boldsymbol{a}_1\left(\boldsymbol{R}\right)\bullet\boldsymbol{d}\left(\boldsymbol{R},\boldsymbol{D}\right)\\
&\left|\boldsymbol{L}_D\left(\boldsymbol{R},\boldsymbol{D}+\boldsymbol{A}\right)-\boldsymbol{a}_2\left(\boldsymbol{R}\right)\right| \approx L_D\left(\boldsymbol{R},\boldsymbol{D}\right)-\boldsymbol{a}_2\left(\boldsymbol{R}\right)\bullet\boldsymbol{d}\left(\boldsymbol{R},\boldsymbol{D}\right)+\boldsymbol{A}\bullet\boldsymbol{d}\left(\boldsymbol{R},\boldsymbol{D}\right)
\end{aligned}
\tag{17}
$$

Hence the complex amplitudes before and after deformation can then be written as:

$$
\begin{aligned}
U_1\left(\boldsymbol{R},\boldsymbol{D}\right) &= \iint\sqrt{I_0\left(\boldsymbol{R}+\alpha_{T1}\left(\boldsymbol{R}\right)\right)}\exp\left(i\phi\right)\\
&\quad\times\exp\left(ik\left[L_S\left(\boldsymbol{R}\right)+L_D\left(\boldsymbol{R},\boldsymbol{D}\right)-\boldsymbol{a}_1\left(\boldsymbol{R}\right)\bullet\boldsymbol{p}\left(\boldsymbol{R},\boldsymbol{D}\right)\right]\right)dxdy\\
U_2\left(\boldsymbol{R},\boldsymbol{D}+\boldsymbol{A}\right) &= \iint\sqrt{I_0\left(\boldsymbol{R}+\alpha_{T2}\left(\boldsymbol{R}\right)\right)}\exp\left(i\phi\right)\\
&\quad\times\exp\left(ik\left[L_S\left(\boldsymbol{R}\right)+L_D\left(\boldsymbol{R},\boldsymbol{D}\right)-\boldsymbol{a}_2\left(\boldsymbol{R}\right)\bullet\boldsymbol{p}\left(\boldsymbol{R},\boldsymbol{D}\right)-\boldsymbol{A}\bullet\boldsymbol{d}\left(\boldsymbol{R},\boldsymbol{D}\right)\right]\right)dxdy
\end{aligned}
\tag{18}
$$

Substituting these expressions into to the cross-correlation of the intensity fluctuation and, as before, setting $\alpha_{T1}(\boldsymbol{R}) = 0$ and $\boldsymbol{a_2}(\boldsymbol{R}) - \boldsymbol{a_1}(\boldsymbol{R}) = \boldsymbol{a}(\boldsymbol{R})$ gives:

$$
\begin{aligned}
\left|\left\langle U_1\left(\boldsymbol{R},\boldsymbol{D}\right)U_2^*\left(\boldsymbol{R},\boldsymbol{D}+\boldsymbol{A}\right)\right\rangle\right| &= \iint\sqrt{I_0\left(\boldsymbol{R}\right)I_0\left(\boldsymbol{R}+\alpha_{T2}\left(\boldsymbol{R}\right)\right)}\\
&\quad\times\exp\left(ik\left[\boldsymbol{p}\left(\boldsymbol{R},\boldsymbol{D}\right)\bullet\boldsymbol{a}\left(\boldsymbol{R}\right)-\boldsymbol{A}\bullet\boldsymbol{d}\left(\boldsymbol{R},\boldsymbol{D}\right)\right]\right)dxdy
\end{aligned}
\tag{19}
$$

However, unlike Eq. (5) in the original derivation above, the further approximations of $\boldsymbol{p}\left(\boldsymbol{R},\boldsymbol{D}+\boldsymbol{A}\right)\bullet\boldsymbol{a}_2\left(\boldsymbol{R}\right) \approx \boldsymbol{p}\left(\boldsymbol{R},\boldsymbol{D}\right)\bullet\boldsymbol{a}_2\left(\boldsymbol{R}\right)$ and the parabolic approximations used to approximate $L_D(\boldsymbol{R},\boldsymbol{D})$ and $L_D(\boldsymbol{R},\boldsymbol{D} + \boldsymbol{A})$ are no longer required. As in Yamaguchi's original derivation, a Taylor series expansion about $\boldsymbol{R} = 0$ and ignoring terms higher than first order is used to expand the $\boldsymbol{p}\left(\boldsymbol{R},\boldsymbol{D}\right)\bullet\boldsymbol{a}\left(\boldsymbol{R}\right)$ term to Eq. (7), and similarly the new $\boldsymbol{A}\bullet\boldsymbol{d}\left(\boldsymbol{R},\boldsymbol{D}\right)$ term is expanded to:

$$
\begin{aligned}
\boldsymbol{A}\bullet\boldsymbol{d}\left(\boldsymbol{R},\boldsymbol{D}\right) &= -A_x d_x\left(\boldsymbol{R},\boldsymbol{D}\right)-A_y d_y\left(\boldsymbol{R},\boldsymbol{D}\right)\\
&\approx -A_x\left(d_x\left(0,\boldsymbol{D}\right)+\left[\nabla d_x\left(\boldsymbol{R},\boldsymbol{D}\right)\right]_0\bullet\boldsymbol{R}\right)-A_y\left(d_y\left(0,\boldsymbol{D}\right)+\left[\nabla d_y\left(\boldsymbol{R},\boldsymbol{D}\right)\right]_0\bullet\boldsymbol{R}\right)\\
&= -\boldsymbol{A}\bullet\boldsymbol{d}\left(0,\boldsymbol{D}\right)-A_x\left[\nabla d_x\left(\boldsymbol{R},\boldsymbol{D}\right)\right]_0\bullet\boldsymbol{R}-A_y\left[\nabla d_y\left(\boldsymbol{R},\boldsymbol{D}\right)\right]_0\bullet\boldsymbol{R}
\end{aligned}
\tag{20}
$$

Substituting Eqs. (7) and (20) into Eq. (19) gives:

$$
\begin{aligned}
\left|\left\langle U_1\left(\boldsymbol{R},\boldsymbol{D}\right)U_2^*\left(\boldsymbol{R},\boldsymbol{D}+\boldsymbol{A}\right)\right\rangle\right| &= \exp\left(ik\left[\boldsymbol{A}\bullet\boldsymbol{d}\left(0,\boldsymbol{D}\right)-\boldsymbol{p}\left(0,\boldsymbol{D}\right)\bullet\boldsymbol{a}\left(0\right)\right]\right)\\
&\quad\times\iint\sqrt{I_0\left(\boldsymbol{R}\right)I_0\left(\boldsymbol{R}+\alpha_{T2}\left(\boldsymbol{R}\right)\right)}\\
&\quad\times\exp\left(ik\begin{bmatrix}-A_x\left[\nabla d_x\left(\boldsymbol{R},\boldsymbol{D}\right)\right]_0-A_y\left[\nabla d_y\left(\boldsymbol{R},\boldsymbol{D}\right)\right]_0\\+\left[\nabla\boldsymbol{p}\left(\boldsymbol{R},\boldsymbol{D}\right)\bullet\boldsymbol{a}\left(\boldsymbol{R}\right)\right]_0\end{bmatrix}\bullet\boldsymbol{R}\right)dxdy
\end{aligned}
\tag{21}
$$

As before, by examining this equation it can be seen that the cross-correlation will be a maximum where the exponential term is zero, hence:

$$
\left[-A_x\left[\nabla d_x\left(\boldsymbol{R},\boldsymbol{D}\right)\right]_0-A_y\left[\nabla d_y\left(\boldsymbol{R},\boldsymbol{D}\right)\right]_0+\left[\nabla\boldsymbol{p}\left(\boldsymbol{R},\boldsymbol{D}\right)\bullet\boldsymbol{a}\left(\boldsymbol{R}\right)\right]_0\right]=0 \tag{22}
$$

Which can be solved to give:

#217014 - $15.00 USD Received 15 Jul 2014; revised 5 Sep 2014; accepted 15 Sep 2014; published 10 Oct 2014
(C) 2014 OSA

$$A_x = \frac{\frac{\delta d_y}{\delta y}\left(\frac{\delta \boldsymbol{p}\bullet\boldsymbol{a}}{\delta x}\right) - \frac{\delta d_y}{\delta x}\left(\frac{\delta \boldsymbol{p}\bullet\boldsymbol{a}}{\delta y}\right)}{\left(\frac{\delta d_x}{\delta x}\frac{\delta d_y}{\delta y} - \frac{\delta d_x}{\delta y}\frac{\delta d_y}{\delta x}\right)} \qquad A_y = \frac{\frac{\delta d_x}{\delta x}\left(\frac{\delta \boldsymbol{p}\bullet\boldsymbol{a}}{\delta y}\right) - \frac{\delta d_x}{\delta y}\left(\frac{\delta \boldsymbol{p}\bullet\boldsymbol{a}}{\delta x}\right)}{\left(\frac{\delta d_x}{\delta x}\frac{\delta d_y}{\delta y} - \frac{\delta d_x}{\delta y}\frac{\delta d_y}{\delta x}\right)} \quad (23)$$

Finally the $\delta \boldsymbol{p}\bullet\boldsymbol{a}/\delta x$ and $\delta \boldsymbol{p}\bullet\boldsymbol{a}/\delta y$ terms can be expanded in terms of the partial derivatives and components of the strain tensor and rotation vector, as in the original derivation. Giving in matrix form:

$$\begin{bmatrix} A_x \\ A_y \end{bmatrix} = [P]\left([T]\begin{bmatrix} a_x \\ a_y \\ a_z \end{bmatrix} + [R]\begin{bmatrix} \Omega_x \\ \Omega_y \\ \Omega_z \end{bmatrix} + [D]\begin{bmatrix} \varepsilon_{xx} \\ \varepsilon_{xy} \\ \varepsilon_{yy} \end{bmatrix} \right) \quad (24)$$

Where:

$$[P] = \frac{1}{\left(\frac{\delta d_x}{\delta x}\frac{\delta d_y}{\delta y} - \frac{\delta d_x}{\delta y}\frac{\delta d_y}{\delta x}\right)}\begin{bmatrix} \frac{\delta d_y}{\delta y} & -\frac{\delta d_y}{\delta x} \\ -\frac{\delta d_x}{\delta y} & \frac{\delta d_x}{\delta x} \end{bmatrix}$$

$$[T] = \begin{bmatrix} \frac{\delta(s_x + d_x)}{\delta x} & \frac{\delta(s_y + d_y)}{\delta x} & \frac{\delta(s_z + d_z)}{\delta x} \\ \frac{\delta(s_x + d_x)}{\delta y} & \frac{\delta(s_y + d_y)}{\delta y} & \frac{\delta(s_z + d_z)}{\delta y} \end{bmatrix}$$

$$[R] = \begin{bmatrix} 0 & -(s_z + d_z) & (s_y + d_y) \\ -(s_z + d_z) & 0 & -(s_x + d_x) \end{bmatrix}$$

$$[D] = \begin{bmatrix} (s_x + d_x) & (s_y + d_y) & 0 \\ 0 & (s_x + d_x) & (s_y + d_y) \end{bmatrix}$$

4.1 Improved equations for the speckle shift from a surface lying in the xy-plane

For the standard case of a plane surface located in the $z = 0$ plane, the partial derivatives given in Eq. (13) can be substituted into the above expressions yielding:

$$[P] = \frac{L_D}{{d_z}^2}\begin{bmatrix} ({d_y}^2 - 1) & -(d_x d_y) \\ -(d_x d_y) & ({d_x}^2 - 1) \end{bmatrix}$$

$$[T] = \begin{bmatrix} \frac{({s_x}^2 - 1)}{L_S} + \frac{({d_x}^2 - 1)}{L_D} & \frac{(s_x s_y)}{L_S} + \frac{(d_x d_y)}{L_D} & \frac{(s_x s_z)}{L_S} + \frac{(d_x d_z)}{L_D} \\ \frac{(s_x s_y)}{L_S} + \frac{(d_x d_y)}{L_D} & \frac{({s_y}^2 - 1)}{L_S} + \frac{({d_y}^2 - 1)}{L_D} & \frac{(s_y s_z)}{L_S} + \frac{(d_y d_z)}{L_D} \end{bmatrix} \quad (25)$$

The result given by Eq. (24) and the matrices [*P*],[*T*] defined in Eq. (25) gives the final expressions for the speckle shift for a mean surface located in the $z = 0$ plane. These match the expressions for speckle shift derived by Jacquot [16] and later by Světlík [17] and for the

#217014 - $15.00 USD Received 15 Jul 2014; revised 5 Sep 2014; accepted 15 Sep 2014; published 10 Oct 2014
(C) 2014 OSA

case of a detector located on the *z*-axis, reduce to those derived by Yamaguchi [1]. Here we have adopted the matrix form used by Světlík for compactness, although it should be noted that there is an apparent typographical error in the [*R*] matrix in Eq. (15) of [17].

4.2 Improved equations for the speckle shift from a shaped/sloped surface

As in section 2.2 this theory can then be extended to include the influence of the surface gradients by substituting the modified partial derivatives given in Eq. (15) into Eq. (24) and rearranging to give:

$$\begin{bmatrix} Ax \\ Ay \end{bmatrix} = [P]\left(\left([T] + [T'] \right) \begin{bmatrix} a_x \\ a_y \\ a_z \end{bmatrix} + [R] \begin{bmatrix} \Omega_x \\ \Omega_y \\ \Omega_z \end{bmatrix} + [D] \begin{bmatrix} \varepsilon_{xx} \\ \varepsilon_{xy} \\ \varepsilon_{yy} \end{bmatrix} \right) \tag{26}$$

Where:

$$[P] = \frac{L_D}{\left({d_z}^2 - m_x d_x d_z - m_y d_y d_z \right)} \begin{bmatrix} \left(m_y d_y d_z + {d_y}^2 - 1 \right) & -\left(m_x d_y d_z + d_y d_x \right) \\ -\left(m_x d_x d_z + d_y d_x \right) & \left(m_x d_x d_z + {d_x}^2 - 1 \right) \end{bmatrix}$$

$$[T] = \begin{bmatrix} \frac{\left({s_x}^2 - 1 \right)}{L_S} + \frac{\left({d_x}^2 - 1 \right)}{L_D} & \frac{\left(s_x s_y \right)}{L_S} + \frac{\left(d_x d_y \right)}{L_D} & \frac{\left(s_x s_z \right)}{L_S} + \frac{\left(d_x d_z \right)}{L_D} \\ \frac{\left(s_x s_y \right)}{L_S} + \frac{\left(d_x d_y \right)}{L_D} & \frac{\left({s_y}^2 - 1 \right)}{L_S} + \frac{\left({d_y}^2 - 1 \right)}{L_D} & \frac{\left(s_y s_z \right)}{L_S} + \frac{\left(d_y d_z \right)}{L_D} \end{bmatrix}$$

$$[T'] = \begin{bmatrix} m_x \left(\frac{s_x s_z}{L_S} + \frac{d_x d_z}{L_D} \right) & m_x \left(\frac{s_y s_z}{L_S} + \frac{d_y d_z}{L_D} \right) & m_x \left(\frac{\left({s_z}^2 - 1 \right)}{L_S} + \frac{\left({d_z}^2 - 1 \right)}{L_D} \right) \\ m_y \left(\frac{s_x s_z}{L_S} + \frac{d_x d_z}{L_D} \right) & m_y \left(\frac{s_y s_z}{L_S} + \frac{d_y d_z}{L_D} \right) & m_y \left(\frac{\left({s_z}^2 - 1 \right)}{L_S} + \frac{\left({d_z}^2 - 1 \right)}{L_D} \right) \end{bmatrix}$$

Where [*T'*] is a matrix relating surface gradients to the additional speckle shift due to surface translations and the matrices [*T*], [*R*], and [*D*] remained unchanged from Eqs. (24) and (26). These expressions derived here for the first time can be seen to reduce to the expressions given in Eq. (25) when the surface gradients (m_x and m_y) are zero, and to the expression given in section 2, when the detector is located on the *z*-axis.

5 Experimental verification of the improved equations

The experimental system and process described in section 3 was used to test the validity of the improved equations given in section 4.1 and 4.2. The results are shown in Fig. 3 and Fig. 4 above and in Figs. 5–8, here. From Fig. 3 it can be seen that the improved theory (solid lines) now successfully predicts the observed translation scaling factors within the tolerances of the measurements (± 0.02) over a wide range of detector positions along the *x*-axis for both zero gradient and sloped surface cases. This is in contrast to the expressions given in section 2.2, using Yamaguchi's original approximations (dashed lines), that fail when the detector is positioned off-axis. It can also be seen that when the detector is positioned on the *z*-axis that the expressions given in sections 4.1 and 4.2 simplify to those given in section 2. Hence the scaling factors predicted by the improved equations are identical to those shown in Fig. 4. To further confirm the validity of the expressions, the scaling factors at three further detector positions, were measured for various surface gradients. The results, shown in Figs. 5–8, are presented in the same manner as Fig. 4, and again show excellent agreement

#217014 - $15.00 USD Received 15 Jul 2014; revised 5 Sep 2014; accepted 15 Sep 2014; published 10 Oct 2014
(C) 2014 OSA

between the experimental and theoretical values. Other detector positions within the range $x,y< \pm$ 80mm have also been investigated and similarly found to be in agreement with the improved theory.

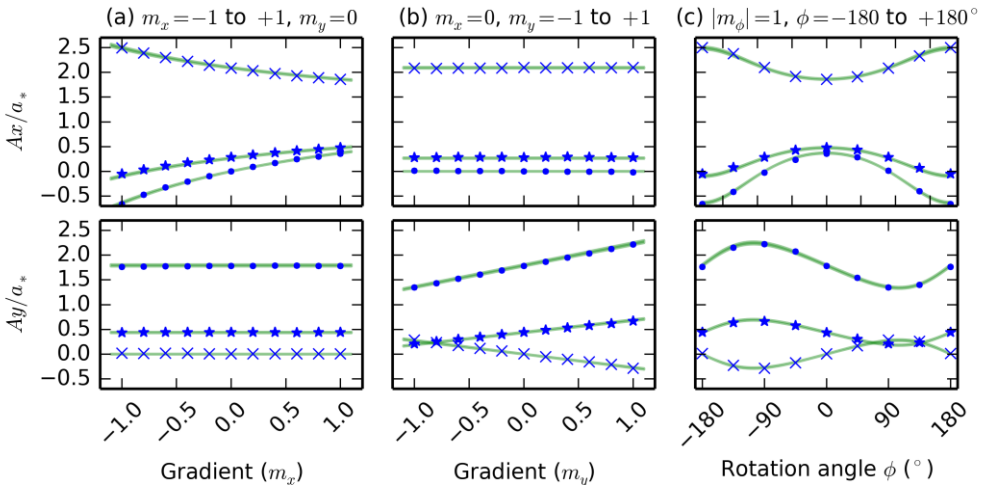


Fig. 5. Comparison of measured and theoretical translational scaling factors for a source and detector positioned at $\boldsymbol{S}$ = (0,-150,265) mm and $\boldsymbol{D}$ = (–80,0,300) mm for varying surface gradients; (a) for varying m_x; (b) for varying m_y and (c) for varying directions of a fixed magnitude gradient as it is rotated about the z-axis (m_x = cosϕ, m_y = -sinϕ). The top row shows the scaling factors for the speckle shift in the x direction (A_x) resulting from the object translations (a_x, a_y and a_z) while the bottom row shows scaling factors for the speckle shift in the y direction (A_y). The data points are the experimentally measured results; (✖)$A_{x,y}/a_x$, (●) $A_{x,y}/a_y$ and (★) $A_{x,y}/a_z$ and the solid lines show the values predicted by the improved equations, presented in section 4. Here the thickness of the line denotes the minimum and maximum bounds predicted assuming an error in source and detector positions of ± 1mm in all directions.

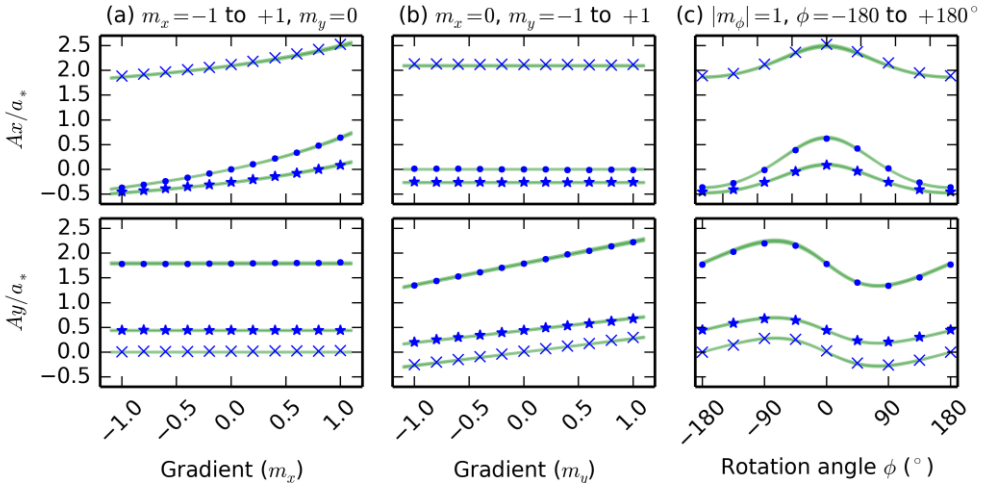


Fig. 6. Comparison of measured and theoretical translational scaling factors for a source and detector positioned at $\boldsymbol{S}$ = (0,-150,265) mm and $\boldsymbol{D}$ = (+ 80,0,300) mm for varying surface gradients; (a) for varying m_x; (b) for varying m_y and (c) for varying directions of a fixed magnitude gradient as it is rotated about the z-axis (m_x = cosϕ, m_y = -sinϕ). The top row shows the scaling factors for the speckle shift in the x direction (A_x) resulting from the object translations (a_x, a_y and a_z) while the bottom row shows scaling factors for the speckle shift in the y direction (A_y). The data points are the experimentally measured results; (✖)$A_{x,y}/a_x$, (●) $A_{x,y}/a_y$ and (★) $A_{x,y}/a_z$ and the solid lines show the values predicted by the improved equations,

#217014 - $15.00 USD Received 15 Jul 2014; revised 5 Sep 2014; accepted 15 Sep 2014; published 10 Oct 2014
(C) 2014 OSA

presented in section 4. Here the thickness of the line denotes the minimum and maximum bounds predicted assuming an error in source and detector positions of ± 1mm in all directions.

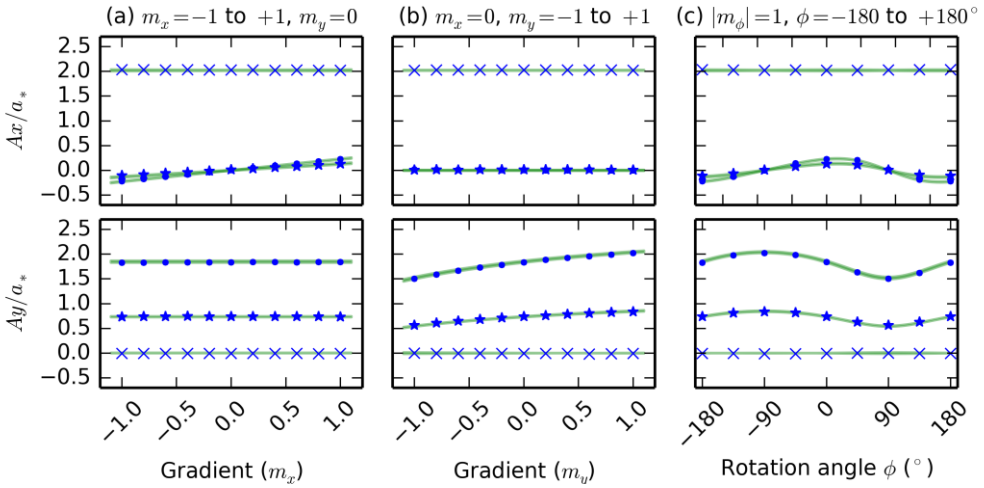


Fig. 7. Comparison of measured and theoretical translational scaling factors for a source and detector positioned at ***S*** = (0,-150,265) mm and ***D*** = (0,-80,300) mm for varying surface gradients; (a) for varying m_x; (b) for varying m_y and (c) for varying directions of a fixed magnitude gradient as it is rotated about the z-axis (m_x = cosϕ, m_y = -sinϕ). The top row shows the scaling factors for the speckle shift in the *x* direction (A_x) resulting from the object translations (a_x, a_y and a_z) while the bottom row shows scaling factors for the speckle shift in the *y* direction (A_y). The data points are the experimentally measured results; (✖)$A_{x,y}/a_x$, (●) $A_{x,y}/a_y$ and (★) $A_{x,y}/a_z$ and the solid lines show the values predicted by the improved equations, presented in section 4. Here the thickness of the line denotes the minimum and maximum bounds predicted assuming an error in source and detector positions of ± 1mm in all directions.

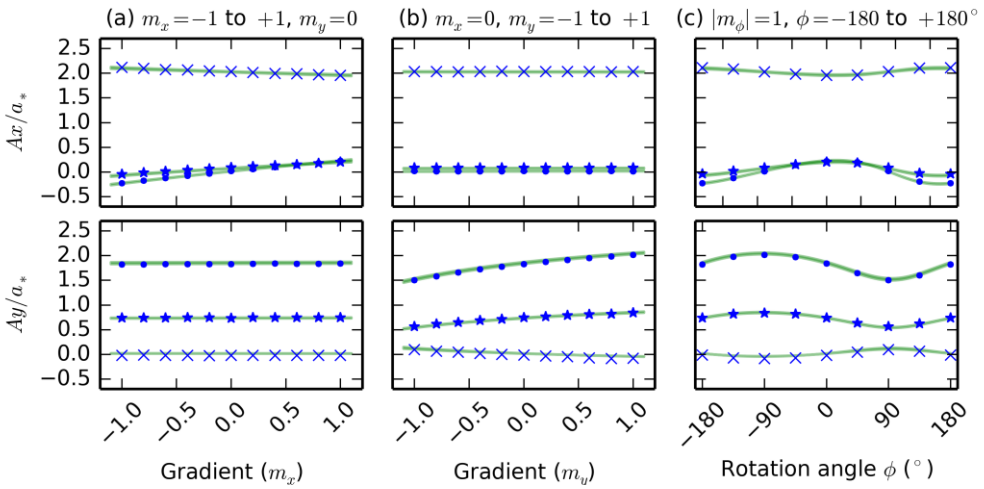


Fig. 8. Comparison of measured and theoretical translational scaling factors for a source and detector positioned at ***S*** = (0,-150,265) mm and ***D*** = (–20,-80,300) mm for varying surface gradients; (a) for varying m_x; (b) for varying m_y and (c) for varying directions of a fixed magnitude gradient as it is rotated about the z-axis (m_x = cosϕ, m_y = -sinϕ). The top row shows the scaling factors for the speckle shift in the *x* direction (A_x) resulting from the object translations (a_x, a_y and a_z) while the bottom row shows scaling factors for the speckle shift in the *y* direction (A_y). The data points are the experimentally measured results; (✖)$A_{x,y}/a_x$, (●) $A_{x,y}/a_y$ and (★) $A_{x,y}/a_z$ and the solid lines show the values predicted by the improved equations, presented in section 4. Here the thickness of the line denotes the minimum and maximum bounds predicted assuming an error in source and detector positions of ± 1mm in all directions.

#217014 - $15.00 USD Received 15 Jul 2014; revised 5 Sep 2014; accepted 15 Sep 2014; published 10 Oct 2014
(C) 2014 OSA

6 Conclusions

Expressions that relate the observed objective speckle shift to the deformation of the illuminated object have been presented and verified experimentally for four cases;

I) A plane surface located in the *xy*-plane, for detectors located on the *z*-axis (section 2.1).

II) A shaped surface approximated by its linear surface gradients, when the detector is located on the *z*-axis (section 2.2).

III) A plane surface located in the *xy*-plane for an arbitrary detector location (section 4.1).

IV) A shaped surface approximated by its linear surface gradients for an arbitrary detector location (section 4.2)

Case I) corresponds to the results given by Yamaguchi [1] and Horvath [19] and is shown experimentally to break down for off-axis detector positions. Case II) corresponds to the theory extended to include surface shape/gradients and is derived here for the first time to our knowledge. It uses the same approximations as Yamaguchi and hence also fails when the detector position is not located on the *z*-axis. However for on-axis detector positions this extended theory can be used to accurately predict speckle shift. For cases III) and IV) improved expressions, that apply over a wider range of detector positions, are derived using a method analogous to Yamaguchi's method, however certain approximations used by Yamaguchi are no longer required. The expression derived for case III), a plane surface located parallel to the xy-plane, agrees with the derivations of Jacquot [16] and Světlík [17] which were found via different routes. Finally, the expression for case IV), a shaped surface approximated by its surface gradients, is derived here for the first time and can be used to predict the speckle translation for a sloped object (Eq. (26) in section 4.2). The new extended and improved expressions are verified by experimental measurements of the in-plane translational scaling factors (the ratio of speckle translation to object translation) for a wide range of sloped surfaces and detector positions.

Acknowledgments

The authors acknowledge the support of the Engineering and Physical Sciences Research Council (EPSRC) UK, via grant EP/H02252X/1 and EP/H019839/1. (For enquiries relating to access to the research data or other materials referred to in this article, please contact Cranfield University Library and Information Services – library@cranfield.ac.uk).



https://dspace.org/

Objective speckle displacement: an extended theory for the small deformation of shaped objects

Charrett, Thomas O. H.; Tatam, Ralph P.

2014-10-10
Optical Society of America
http://dx.doi.org/10.1364/OE.22.025466
Thomas O. H. Charrett and Ralph P. Tatam. (2014). Objective speckle displacement: an extended theory for the small deformation of shaped objects. Optics Express, Vol. 22, Issue 21, pp. 25466-25480.

Downloaded from a DSpace repository. https://dspace.org/